Space Weather

Key Points:
- Heliographic latitudinal offset can have a significant effect on corotation solar wind forecasting from L5
- The error introduced by latitudinal offset is maximized at solar minimum and during the solstices
- A combination of L5 measurements and global MHD modeling may yield the most accurate solar wind forecasts

Correspondence to:
M. J. Owens,
m.j.owenst@reading.ac.uk

Near-Earth Solar Wind Forecasting Using Corotation From L5: The Error Introduced By Heliographic Latitude Offset

M. J. Owens[1] , P. Riley[2] , M. Lang[3] , and M. Lockwood[1]

[1]Department of Meteorology, University of Reading, Berkshire, UK, [2]Predictive Science Inc., San Diego, CA, USA, [3]Le Laboratoire des Sciences du Climat et de l'Environnement, CEA-CNRS-UVSQ, Gif Sur Yvette, France

Abstract Routine in situ solar wind observations from L5, located 60° behind Earth in its orbit, would provide a valuable input to space weather forecasting. One way to utilize such observations is to assume that the solar wind is in perfect steady state over the 4.5 days it takes the Sun to rotate 60°, and thus, near-Earth solar wind in 4.5 days time would be identical to that at L5 today. This corotation approximation is most valid at solar minimum when the solar wind is slowly evolving. Using STEREO data, it has been possible to test L5-corotation forecasting for a few months mostly at solar minimum, but the various contributions to forecast error cannot be disentangled. This study uses 40+ years of magnetogram-constrained solar wind simulations to isolate the effect of latitudinal offset between L5 and Earth due to the inclination of the ecliptic plane to the solar rotational equator. Latitudinal offset error is found to be largest at solar minimum, due to the latitudinal ordering of solar wind structure. It is also a strong function of time of year: maximum at the solstices and very low at equinoxes. At solstice, the latitudinal offset alone means L5-corotation forecasting is expected to be less accurate than numerical solar wind models, even before accounting for time-dependent solar wind structures. Thus, a combination of L5-corotation and numerical solar wind modeling may provide the best forecast. These results also highlight that three-dimensional solar wind structure must be accounted for when performing solar wind data assimilation.

Plain Language Summary The solar wind is a continuous outflow of electrically charged material driven by the Sun's magnetic field. Variability in solar wind conditions give rise to hazardous "space weather." One way to forecast solar wind conditions is by assuming the Sun's magnetic field is constant and therefore that same conditions at Earth will repeat every solar rotation (27 days). In reality, the Sun's field changes significantly over 27 days, particularly at solar maximum. An improved forecast may be provided by a space weather mission to L5, a gravitationally stable position 60° behind Earth in its orbit. A spacecraft at L5 would observe the solar wind expected to rotate to Earth only 4.5 days later. However, Earth's orbit is slightly misaligned with the solar rotational equator. Thus L5 and Earth are generally at different solar latitudes. While this difference is small—around 7° at most—it can still be important. We use 40 years of solar wind simulations to show that the largest forecast errors occur around the solstices and are negligible at the equinoxes. Somewhat counterintuitively, the latitudinal-forecast error is significantly larger at solar minimum than at solar maximum. This is because the solar wind is primarily structured in latitude at solar minimum.

1. Introduction

Space weather can disrupt power grids, communications, and satellite operations and poses a threat to health of humans in space and on high-altitude aircraft (Cannon et al., 2013). Long lead time (>1 day) space weather forecasting requires accurate prediction of near-Earth solar wind conditions. For this purpose, U.K. and U.S. forecast centers primarily use numerical magnetohydrodynamic (MHD) coronal and solar wind models constrained by observations of the photospheric magnetic field (Odstrcil, 2003; Riley et al., 2001; Tóth et al., 2005). Transient structures resulting from coronal mass ejections (CMEs), can be inserted into numerical solar wind models (Odstrcil et al., 2004). Nevertheless, simple empirical solar wind forecasts can serve as useful independent forecasts, as well as providing a contingency if, for example, magnetogram observations are not available (Owens, Riley, et al., 2017).

One such empirical forecast method is solar wind recurrence (sometimes referred to as 27-day persistence), which assumes corotation of steady-state or quasi-steady-state solar wind structures. It predicts that the near-Earth solar wind in one solar rotation's time (approximately 27.27 days relative to Earth's motion) will be the same as that today. This works well for heliospheric magnetic field (HMF) polarity and solar wind speed (V_R) at solar minimum, often outperforming the MHD models (Owens et al., 2013) for the ambient solar wind. Except for rare cases when long-lived active regions introduce 27-day periodicity by producing multiple CMEs over multiple rotations, recurrence is not capable of forecasting transient CMEs. Toward solar maximum, however, the corona becomes increasingly dynamic and transient CMEs make up an increasing proportion of the solar wind (Cane & Richardson, 2003; Riley, 2007). Thus, the steady-state assumption over 27 days becomes increasingly invalid and recurrence forecasting performs poorly (Owens et al., 2013). Information about the time evolution of the corona can be incorporated to improve recurrence forecasts (Temmer et al., 2018).

A proposed operational space weather mission (Hapgood, 2017) at the Lagrange L5 point, 60° behind Earth in its orbit, provides an opportunity to make a corotation forecast with a much shorter (4.5 days) assumption of steady-state conditions (Miyake et al., 2005). Such advanced knowledge of steady-state solar wind structures is expected to have wide-ranging space-weather applications (McGranaghan et al., 2014).

The STEREO mission Kaiser (2005), with two spacecraft in Earth-like orbits but drifting ahead and behind Earth at a rate of 22.5° per year, provided a unique opportunity to test a corotation forecast from L5 (Simunac et al., 2009; Turner & Li, 2011); the STEREO spacecraft were separated from each other by 60° longitude in early 2008, and from Earth by 60° near the end of 2009. During these few months of data during a particularly deep solar minimum, L5 corotation was shown to be superior to a 27-day recurrence forecast from near-Earth data (Kohutova et al., 2016). The improvement, however, was fairly modest, with only ∼20% skill gain in solar wind speed forecast relative to 27-day recurrence (Kohutova et al., 2016; Thomas et al., 2018). As the STEREO spacecraft approached the far side of the Sun (from Earth's viewpoint), they again achieved a brief 60° separation in December 2013. During this time there was considerable difference in the solar wind structures (Jian et al., 2019).

Limitations on L5-corotation forecasting likely include the following: (1) transient CMEs, which only encounter either L5 or Earth; (2) evolution of the large-scale solar wind structures over the 4.5-day corotation period; (3) small-scale stochastic processes such as solar wind turbulence (Bruno & Carbone, 2005); and (4) the heliographic latitudinal offset of L5 relative to Earth resulting from the inclination of the ecliptic plane to the solar rotation axis. From the few months of L5-like STEREO data it is not possible to disentangle these effects. The latitudinal offset was small amplitude, varying between 0° and 7° over the year. Global solar wind simulations, however, suggest that even small latitudinal variations can have a considerable effect on the solar wind structures encountered (Riley et al., 2010).

In this study, we use coupled coronal and heliospheric simulations, constrained by photospheric magnetic field observations, to produce completely steady-state reconstructions of the solar wind. By sampling L5 and Earth-like trajectories through the 1-AU solar wind structure, we isolate and quantify the effect of the L5-Earth heliolatitude offset for a range of solar activity levels.

2. Data

Solar wind structure is determined using the MHD algorithm outside a sphere (MAS) global coronal and heliosphere model (Linker et al., 1999; Riley et al., 2012). MAS is constrained by photospheric magnetic field observations, which are computed outward to 30 solar radii, while self-consistently solving the plasma and magnetic field parameters on a nonuniform grid in polar coordinates, using the MHD equations and the vector potential **A** (where the magnetic field, **B**, is given by $\nabla \times A$, such that $\nabla \cdot \nabla \times A = 0$, which ensures current continuity, $\nabla \cdot J = 0$, is conserved to within the model's numerical accuracy). The heliospheric version of MAS then propagates solar wind conditions out to 1 AU. We use MAS solutions based on Carrington maps of the photospheric magnetic field and thus assume that the solar wind is completely steady state over a Carrington rotation (CR). Magnetograms from a range of observatories are used to minimize data gaps and provide the longest possible time sequence. See Owens, Lockwood, et al. (2017) for details of the data set. The heliospheric MAS used in this study is based on the polytropic approximation (Linker et al., 1999) and uses a grid resolution of 121, 128, and 140 cells in the meridional, azimuthal, and radial directions, respectively. As steady-state solar wind is assumed and the time series at 1 AU is produced by rotation, the

effective time resolution is set by the azimuthal resolution of MAS. In this case, the effective time resolution is approximately 5 hr.

The use of the MAS solar wind solutions in this study does not require the model to accurately forecast or reconstruct specific solar wind intervals. For the purposes of this study, we are only reliant on MAS reproducing the solar wind speed structures and the position of the heliospheric current sheet (HCS) in a statistical sense. Specifically, we require accurate representation of the latitudinal width of the slow wind band, and the shape and inclination to the rotational axis of the slow wind band and HCS. These features control the proportions and durations of fast/slow wind and inward/outward magnetic sectors in the ecliptic plane and thus whether spacecraft at Earth and L5 are likely to observe the same solar wind features. We note that even a systematic bias in the reconstructed solar wind speed would not necessary be an issue for the results presented here, as only the difference between L1 and L5 latitudes is considered.

The width of the slow solar wind band predicted from the MAS model has been shown to provide good agreement with the three Ulysses fast latitude scans under differing solar activity levels (Jian et al., 2011, 2016; Owens, Lockwood, et al., 2017). The latitudinal extent of slow wind predicted by MAS and observed using interplanetary scintillation is also in reasonable agreement (e.g., qualitatively comparing Figure 6 of Manoharan, 2012, and Figure 4a of Owens, Lockwood, et al., 2017). The proportions of fast and slow wind seen in the ecliptic are generally well reproduced by magnetogram extrapolations when the estimated speed is a function of both the expansion factor of a magnetic flux tube between the photosphere and the source surface, and the distance of the flux tube from the coronal hole boundary, as is the case with MAS (McGregor et al., 2011; Riley et al., 2015). Thus the relative occurrence of fast/slow streams near the ecliptic plane is reasonably well reproduced in a point-by-point manner (Jian et al., 2015; Owens et al., 2008; Riley et al., 2010). Taking a feature-based approach by identifying high-speed enhancements in model and observations and allowing for timing errors, which are not critical to the present study (Owens et al., 2005), MAS produces good agreement with observations, once transient solar wind structures are discounted (Jian et al., 2015, 2016; Owens et al., 2008).

Ulysses observations of the latitudinal extent of the HCS are well reproduced by magnetogram-constrained models such as MAS (e.g., see Figure 13 in Owens and Forsyth, 2013). This is also true in the ecliptic plane, with a strong correspondence between magnetogram-based models and in situ magnetic sector structure, even at solar maximum (e.g., see Figure 5 in Owens and Forsyth, 2013).

Given models such as MAS generally produce "smoother" solar wind speed and HMF structures than those observed, the differences between L5 and Earth are likely to be underestimated. Therefore, the values estimated in this study should be treated as a lower limit.
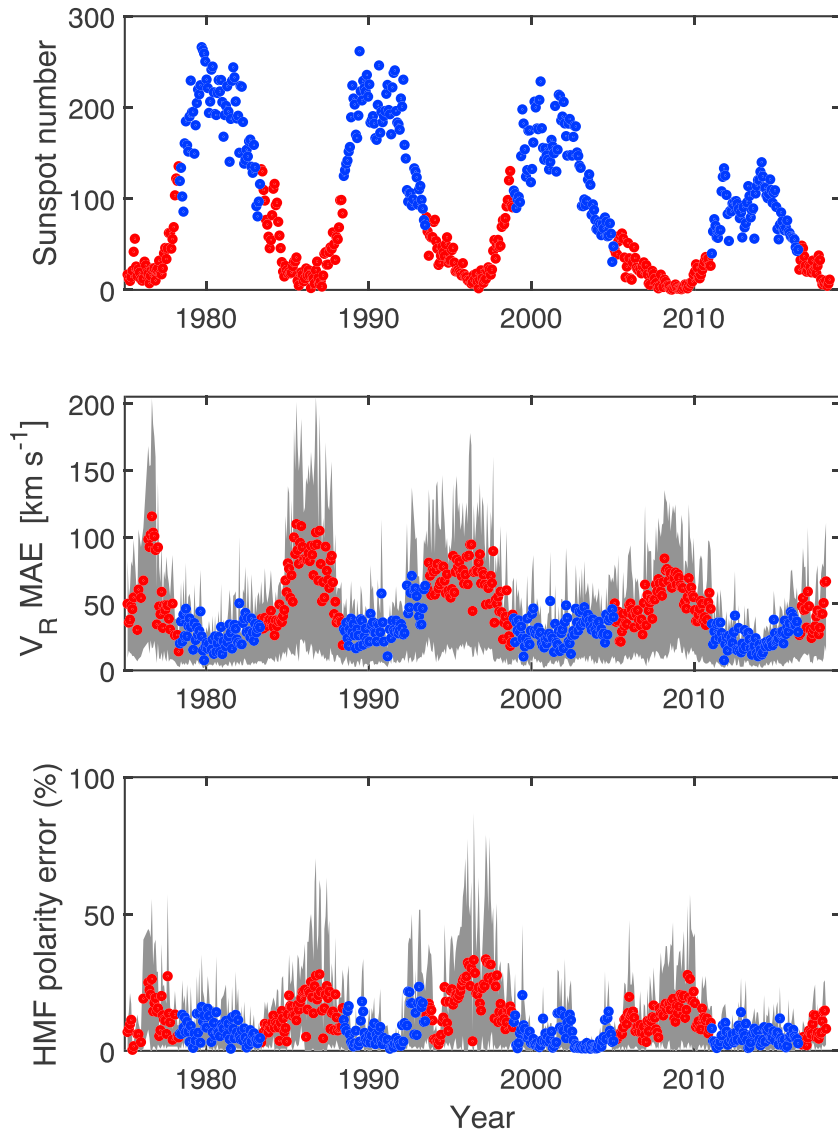
3. Results

Examples of 1-AU solar wind structure are shown in Figure 1. For the solar minimum example (CR1914), slow wind is confined to the equatorial region, while fast wind fills the heliosphere for latitudes more than 25° from the equator. The latitudinal gradients in solar wind speed are large close to the equator (and ecliptic plane). Similarly, the HCS lies very close the equator. While CR 1914 spanned mid-September to mid-October 1996, we consider how the corotation forecast would have fared if such a solar wind configuration was encountered in June. Around the summer solstice, Earth lies close to the helioequator and consequently remains primarily within the slow solar wind, except for a moderate increase in solar wind speed around 230° Carrington longitude. Earth crosses the HCS three times and thus sees four different magnetic sectors. That the polarity of the field at Earth on either side of the HCS reflects that of solar polar field was first noted by Rosenberg and Coleman (1969) and this "Rosenberg-Coleman effect" means that L5 and Earth will see opposite polarity HMF when their difference in heliographic latitudes places them on opposite sides of the HCS. The time Earth spends above/below the HCS in Figure 1 is approximately equal, resulting in roughly equal proportions of inward and outward polarity HMF. Conversely, L5 is well below the equator during June, approximately −6.5° to −4.5° heliolatitude. As a result, L5 encounters significantly more fast wind than Earth, particularly around Carrington longitudes of 0° to 80°, and L5 remains predominantly below the HCS and thus sees primarily inward polarity HMF. Thus, if near-Earth conditions were predicted using L5 corotation for this solar wind configuration during June, the mean absolute error (MAE) in V_R would be 106 km/s and the HMF polarity would be incorrect 44% of the time.
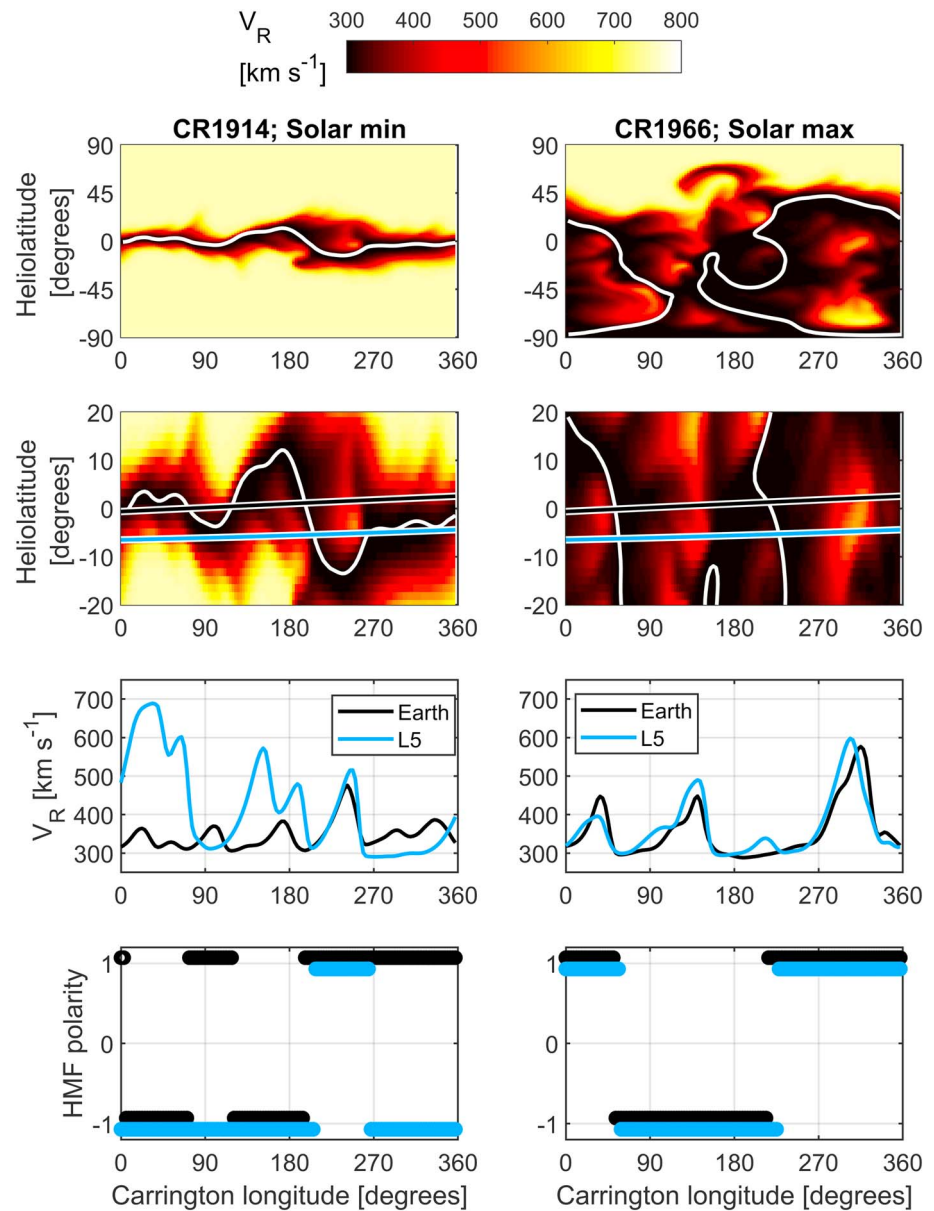
Figure 1. Examples of 1-AU solar wind structure from solar minimum (left column) and solar maximum (right column). (top row) The global solar wind structure at 1 AU, shown as a heliolatitude-Carrington longitude map. The color map extends from 300 (black) to 800 km/s (white). The white line shows the heliospheric current sheet. (second row) Same as top but with latitude restricted to 20° about the equator. Black and blue lines show paths of Earth and L5, respectively, if these solar wind structures had been encountered in June. (third row) Solar wind speed at Earth (black) and L5 (blue). (bottom row) Heliospheric magnetic field polarity in the same format. HMF = heliospheric magnetic field.

At solar maximum (CR1966, approximately spanning August 2000), the picture is very different. Slow solar wind dominates, with fast wind confined to the north pole (at latitudes above 45°). Within 20° of the equator, the latitudinal speed gradients are greatly reduced compared to the solar minimum case, and the HCS is essentially vertical. As a result, L5 and Earth see almost identical solar wind conditions, and a corotation forecast would give a V_R MAE of only 26 km/s and only 5% of the HMF polarities would be incorrect. Of course, these errors are purely for the latitudinal offset between L5 and Earth and at solar maximum the corona is far more dynamic. Thus the steady-state assumption would become the primary source of error in a L5-corotation forecast at this time.
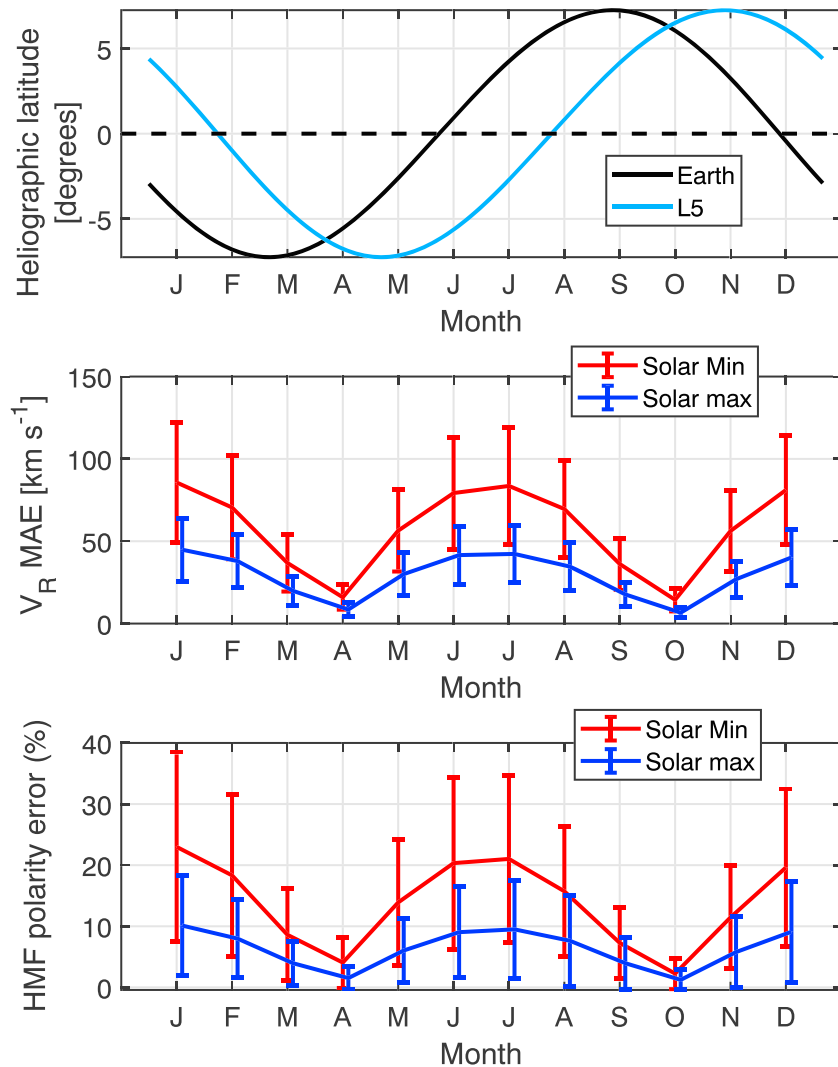
Figure 2. Time series of L5-corotation prediction error resulting purely from latitudinal offsets between L5 and Earth. All data are Carrington rotation averages with red and blue indicating solar minimum and maximum, respectively, based on the phase of the solar cycle. (top) Sunspot number. (middle) MAE in near-Earth V_R based on corotation from L5. We compute MAE for Earth and L5 latitudes during the 12 calendar months. Colored dots show the mean value for all months, and the shaded area spans the maximum and minimum values. (bottom) The percentage of incorrect magnetic polarity intervals, in the same format as the middle panel. HMF = heliospheric magnetic field; MAE = mean absolute error.

We extend this analysis to a statistical study using all CRs from early 1975 to mid-2018 (CR 1625 to 2203). This spans four sunspot cycles, as shown by the upper panel of Figure 2. For each CR, we consider how the L5-corotation forecast would vary with time of year. The annual variation in heliolatitude of L5 and Earth is shown in the top panel of Figure 3. It can be seen that monthly sampling of the heliolatitudes of Earth and L5 gives full coverage of the latitidual offsets between the two positions. Thus, for each CR, we sample the L5 and Earth latitudes using the latitudinal positions for each individual calendar month.

Figure 2 shows the time series of L5 corotation errors purely from latitudinal offset. As expected from the two example CRs shown in Figure 1, on average the V_R MAE is maximized around solar minimum and minimized at solar maximum (very similar trends are found for other metrics, such as root-mean-square error). The percentage of incorrect magnetic polarity intervals follows the same basic trend. For a given CR, there is a large spread in the V_R and magnetic polarity error depending on the month at which the

Figure 3. The annual variation in L5-corotation prediction error resulting purely from latitudinal offsets between L5 and Earth. (top) The heliographic latitude of L5 (blue) and Earth (black) over the year. (middle) V_R MAE as a function of time of year for solar minimum (red) and solar maximum (blue). The line shows the mean of all Carrington rotations, while the error bar is one standard deviation. (bottom) The percentage of incorrect HMF polarities, in the same format. HMF = heliospheric magnetic field; MAE = mean absolute error.

prediction is made. For example, during 1986, the mean V_R MAE is approximately 100 km/s, but the range spans 20 to 190 km/s. In 1996 the average percentage of incorrect HMF polarities is approximately 30%, but the range spans 0% to more than 75% (i.e., significantly worse than random chance). We also note long-term trends, with both peak and mean values of V_R MAE reduced in the most recent solar minimum (2008–2010) compared with the three previous minima.

Figure 3 shows that the large spread in forecast errors for a given CR is a result of the large annual variation in heliolatitude offset between L5 and Earth. CRs are split into solar minimum and maximum periods on the basis of the solar cycle phase. This is deemed preferable to using a simple sunspot number threshold, as that would select different proportions of small/large sunspot cycles. We use solar cycle phase limits of 0.17 and 0.67 of the way through the cycle from solar minimum (Owens et al., 2011), which both splits the data set in half and selects similar sunspot number gradients in the rise and declining phase of each cycle (but allows for changing magnitude of cycles). At solar minimum during the solstices, the V_R MAE is 80 ± 30 km/s. During the equinoxes, however, this drops to 20 ± 11 km/s. For the HMF polarity, 23 ± 16% of intervals are incorrect at solstices, dropping to 5 ± 4% at equinoxes.

4. Conclusions

Near-Earth solar wind can be forecast from in situ L5 observations by assuming the solar wind is steady state over the 4.5 days it takes structures to rotate between the two positions (Kohutova et al., 2016; Miyake et al., 2005; Thomas et al., 2018). Such L5-corotation forecasting will undoubtedly be a useful additional tool in space weather prediction. However, there are inherent limitations to the skill of such forecasts, not only from the steady-state assumption and existence of transient solar wind structures but also from the heliographic latitudinal difference resulting from the inclination of the ecliptic plane to the solar rotational equator. Isolating and quantifying the contributions of these effects is difficult with the limited solar wind data from L5 (or L5-like longitudinal spacecraft separations) presently available.

In this study we have used magnetogram-constrained simulations of the solar wind over the last 40+ years to isolate and quantify the latitudinal offset effect. The latitudinal separation of L5 and Earth has the largest influence on corotation forecasting at solar minimum, when the solar wind is latitudinally structured, and during the summer and winter soltices (December/January and June/July). At solar maximum, when solar wind features are more longitudinally structured, and during the equinoxes, the effect of latitudinal offset is reduced. However, at solar maximum the steady-state approximation breaks down and reduces the usefulness of L5-corotation forecasting.

Comparing the last four solar minima, the STEREO/ACE L5-analogous periods from 2008 and late 2009 may not be representative of the skill of corotation forecasting in general. The average V_R MAE owing to latitudinal offset in the deep 2008–2010 minimum was reduced compared with previous minima (by approximately 25%). This is likely to be the result of the 2008–2010 minimum producing a broader slow wind band than previous minima, meaning the latitudinal gradient in solar wind speed near the helioequator is reduced (Owens et al., 2014).

At solar minimum, the expected V_R MAE for L5-corotation forecasts ranges from approximately 20 km/s at the equinoxes to 80 km/s at the solstices. This is purely from the latitudinal offset and, in practice, will be the lower limit with additional error introduced by time-dependent solar wind structures and transient CMEs, which are only seen (or are different) at either L5 or Earth. As a comparison, steady-state magnetogram-constrained numerical MHD solar wind models have been shown to produce MAE errors in V_R of around 70–80 km/s (Owens et al., 2008). This estimate, however, is from comparison with real solar wind observations and thus does include time evolution, turbulence and CMEs. For the HMF polarity, L5 corotation is expected to produce incorrect polarities around 25% of the time at the solstices but correctly predict the polarity around 95% of the time at the equinoxes. Thus, a hybrid scheme may be the best forecasting approach, wherein L5 corotation are preferentially weighted at equinox and numerical solar wind models are preferentially weighted at solstice. Such a hybrid scheme could be based upon data assimilation (DA) (Lang et al., 2017) that combines the observations, at L5, with a numerical solar wind forecasting model in order to optimally estimate the solar wind at Earth.

Note that the HMF polarity error in corotation predictions from L5 data will have complex effects on predictions of geoeffectiveness because of the influence of the north-south component of the field in the geocentric solar magnetospheric (GSM) frame of reference ($[B_z]_{GSM}$), which predicts the magnetic shear across the dayside boundary of the magnetosphere and so the degree to which the transfer into the terrestrial magnetosphere of solar wind mass, momentum, and energy can occur. This is a complex mixture of the "Rosenberg-Coleman" (RC) and "Russell-McPherron" (RM) effects (Rosenberg & Coleman, 1969; Russell & McPherron, 1973). The RC effect means that the latitude difference between L5 and Earth can cause a difference in the polarities of $[B_x]_{GSE}$ (toward, radial in the geocentric solar ecliptic [GSE] frame) component at the two sites and this would generally give a difference in the $[B_y]_{GSE}$ component because the dominant gardenhose HMF orientation of the Parker spiral means that $[B_y]_{GSE}/[B_x]_{GSE} < 0$. The RM effect is where the $[B_y]_{GSE}$ component of the HMF yields a $[B_z]_{GSM}$ component because of the angle between the GSE and GSM frames. This angle has an annual and a diurnal variation due to, respectively, the angle between the Earth's rotational axis and the X direction of the GSE frame and due to the offset between Earth's rotational and magnetic axes (Lockwood et al., 2016). Specifically, southward HMF in the GSM frame is generated around the March equinox (peaking at 20 UT) when $[B_y]_{GSE} < 0$ (i.e., $[B_x]_{GSE} > 0$) and around the September equinox (peaking at 10 UT) when $[B_y]_{GSE} > 0$ (i.e., $[B_x]_{GSE} < 0$). Although this RC-RM effect introduces quite a lot of diversity into the difference in geoeffectiveness between the solar wind/HMF seen at Earth

and L5 when the polarities of the radial HMF at Earth and L5 are different, that diversity is systematic with time of year and UT and so is relatively easily predicted.

In addition to corotation forecasting, in situ solar wind observations from L5 would enable improvement of numerical solar wind forecasting via DA. DA is the merging of model and observational data to ensure an optimal estimate for reality. Forecast skill has been improved via DA using L5-like observations with a two-dimensional solar wind model (Lang & Owens, 2019). In standard L5-corotation forecasts, the observation is assumed to be "truth," in that it contains no errors. Figure 3 shows one example of why this is not always the case; L5 can be sampling solar wind from a latitude that is not representative of the solar wind at Earth. DA allows estimates of the solar wind to be modified to account for observation errors present as a result of incorrect modeling/assumptions (e.g., assuming that the observations have no latitudinal offset). The results presented here also suggest that L5 DA would benefit greatly from use with fully three-dimensional solar wind models.

References

Bruno, R., & Carbone, V. (2005). The solar wind as a turbulence laboratory. *Living Reviews in Solar Physics*, *10*, 208.

Cane, H. V., & Richardson, I. G. (2003). Interplanetary coronal mass ejections in the near-Earth solar wind during 1996–2002. *Journal of Geophysical Research*, *108*(A4), 1156. https://doi.org/10.1029/2002JA009817

Cannon, P., Angling, M., Barclay, L., Curry, C., Dyer, C., Edwards, R., et al. (2013). *Extreme space weather: Impacts on engineered systems and infrastructure*. London: Royal Academy of Engineering.

Hapgood, M. (2017). L1L5Together: Report of workshop on future missions to monitor space weather on the Sun and in the solar wind using both the L1 and L5 Lagrange points as valuable viewpoints. *Space Weather*, *15*, 654–657. https://doi.org/10.1002/2017SW001652

Jian, L. K., Luhmann, J. G., Russell, C. T., & Galvin, A. B. (2019). Solar Terrestrial Relations Observatory (STEREO) observations of stream interaction regions in 2007–2016: Relationship with heliospheric current sheets, solar cycle variations, and dual observations. *Solar Physics*, *294*(3), 31. https://doi.org/10.1007/s11207-019-1416-8

Jian, L. K., MacNeice, P. J., Mays, M. L., Taktakishvili, A., Odstrcil, D., Jackson, B., et al. (2016). Validation for global solar wind prediction using Ulysses comparison: Multiple coronal and heliospheric models installed at the Community Coordinated Modeling Center. *Space Weather*, *14*, 592–611. https://doi.org/10.1002/2016SW001435

Jian, L. K., MacNeice, P. J., Taktakishvili, A., Odstrcil, D., Jackson, B., Yu, H.-S., et al. (2015). Validation for solar wind prediction at Earth: Comparison of coronal and heliospheric models installed at the CCMC. *Space Weather*, *13*, 316–338. https://doi.org/10.1002/2015SW001174

Jian, L. K., Russell, C. T., Luhmann, J. G., MacNeice, P. J., Odstrcil, D., Riley, P., et al. (2011). Comparison of observations at ACE and Ulysses with Enlil model results: Stream interaction regions during Carrington rotations 20162018. *Solar Physics*, *273*(1), 179–203. https://doi.org/10.1007/s11207-011-9858-7

Kaiser, M. L. (2005). The STEREO mission: An overview. *Advances in Space Research*, *36*(8), 1483–1488. Retrieved from https://www.sciencedirect.com/science/article/pii/S0273117705000505?via%3Dihub, https://doi.org/10.1016/J.ASR.2004.12.066

Kohutova, P., Bocquet, F.-X., Henley, E. M., & Owens, M. J. (2016). Improving solar wind persistence forecasts: Removing transient space weather events, and using observations away from the Sun-Earth line. *Space Weather*, *14*, 802–818. https://doi.org/10.1002/2016SW001447

Lang, M., Browne, P., van Leeuwen, P. J., & Owens, M. (2017). Data assimilation in the solar wind: Challenges and first results. *Space Weather*, *15*, 1490–1510. https://doi.org/10.1002/2017SW001681

Lang, M., & Owens, M. J. (2019). A variational approach to data assimilation in the solar wind. *Space Weather*, *17*, 59–83. https://doi.org/10.1029/2018SW001857

Linker, J., Mikic, Z., Biesecker, D. A., Forsyth, R. J., Gibson, W. E., Lazarus, A. J., et al. (1999). Magnetohydrodynamic modeling of the solar corona during whole Sun month. *Journal of Geophysical Research*, *104*, 9809–9830.

Lockwood, M., Owens, M. J., Barnard, L. A., Bentley, S., Scott, C. J., & Watt, C. E. (2016). On the origins and timescales of geoeffective IMF. *Space Weather*, *14*, 406–432. https://doi.org/10.1002/2016SW001375

Manoharan, P. K. (2012). Three-dimensional evolution of solar wind during solar cycles 22–24. *The Astrophysical Journal*, *751*(2), 128–141. https://doi.org/10.1088/0004-637X/751/2/128

McGranaghan, R., Knipp, D. J., McPherron, R. L., & Hunt, L. A. (2014). Impact of equinoctial high-speed stream structures on thermospheric responses. *Space Weather*, *12*, 277–297. https://doi.org/10.1002/2014SW001045

McGregor, S. L., Hughes, W. J., Arge, C. N., Owens, M. J., & Odstrcil, D. (2011). The distribution of solar wind speeds during solar minimum: Calibration for numerical solar wind modeling constraints on the source of the slow solar wind. *Journal of Geophysical Research*, *116*, A03101. https://doi.org/10.1029/2010JA015881

Miyake, W., Saito, Y., Hayakawa, H., & Matsuoka, A. (2005). On the correlation of the solar wind observed at the L5 point and at the Earth. *Advances in Space Research*, *36*(12), 2328–2332. https://www.sciencedirect.com/science/article/pii/S0273117705004552?via%3Dihub, https://doi.org/10.1016/J.ASR.2004.06.019

Odstrcil, D. (2003). Modeling 3-D solar wind structures. *Advances in Space Research*, *32*, 497–506.

Odstrcil, D., Riley, P., & Zhao, X.-P. (2004). Numerical simulation of the 12 May 1997 interplanetary CME event. *Journal of Geophysical Research*, *109*, A02116. https://doi.org/10.1029/2003JA010135

Owens, M. J., Arge, C. N., Spence, H. E., & Pembroke, A. (2005). An event-based approach to validating solar wind speed predictions: high-speed enhancements in the Wang-Sheeley-Arge model. *Journal of Geophysical Research*, *110*, A12105. https://doi.org/10.1029/2005JA011343

Owens, M. J., Challen, R., Methven, J., Henley, E., & Jackson, D. R. (2013). A 27 day persistence model of near-Earth solar wind conditions: A long lead-time forecast and a benchmark for dynamical models. *Space Weather*, *11*, 225–236. https://doi.org/10.1002/swe.20040

Owens, M. J., Crooker, N. U., & Lockwood, M. (2014). Solar cycle evolution of dipolar and pseudostreamer belts and their relation to the slow solar wind. *Journal of Geophysical Research: Space Physics*, *119*, 36–46. Retrieved from http://adsabs.harvard.edu/abs/2014JGRA.. 119...36O, https://doi.org/10.1002/2013JA019412

Owens, M. J., & Forsyth, R. J. (2013). The heliospheric magnetic field. *Living Reviews in Solar Physics*, *10*, 5. https://doi.org/10.12942/ lrsp-2013-5

Owens, M. J., Lockwood, M., Barnard, L., & Davis, C. J. (2011). Solar cycle 24: Implications for energetic particles and long-term space climate change. *Geophysical Research Letters*, *38*, L19106. https://doi.org/10.1029/2011GL049328

Owens, M. J., Lockwood, M., & Riley, P. (2017). Global solar wind variations over the last four centuries. *Scientific Reports*, *7*, 41548. https:// doi.org/10.1038/srep41548

Owens, M. J., Riley, P., & Horbury, T. (2017). The role of empirical space-weather models (in a world of physics-based numerical simulations). *Proceedings of the International Astronomical Union*, *13*(S335), 254–257. Retrieved from https://www.cambridge.org/core/ product/identifier/S1743921317007128/type/journal_article, https://doi.org/10.1017/S1743921317007128

Owens, M. J., Spence, H. E., McGregor, S., Hughes, W. J., Quinn, J. M., Arge, C. N., et al. (2008). Metrics for solar wind prediction models: Comparison of empirical, hybrid, and physics-based schemes with 8 years of L1 observations. *Space Weather The International Journal Of Research And Applications*, *6*(8), S08001. https://doi.org/10.1029/2007SW000380

Riley, P. (2007). An alternative interpretation of the relationship between the inferred open solar flux and the interplanetary magnetic field. *The Astrophysical Journal*, *667*, L97–L100. https://doi.org/10.1086/522001

Riley, P., Linker, J. A., & Arge, C. N. (2015). On the role played by magnetic expansion factor in the prediction of solar wind speed. *Space Weather*, *13*, 154–169. https://doi.org/10.1002/2014SW001144

Riley, P., Linker, J. A., Lionello, R., & Mikic, Z. (2012). Corotating interaction regions during the recent solar minimum: The power and limitations of global MHD modeling. *Journal of Atmospheric and Solar-Terrestrial Physics*, *83*, 1–10. Retrieved from http://www.sciencedirect. com/science/article/pii/S1364682611003464, https://doi.org/10.1016/j.jastp.2011.12.013

Riley, P., Linker, J. A., & Mikic, Z. (2001). An empirically-driven global MHD model of the solar corona and inner heliosphere. *Journal of Geophysical Research*, *106*, 15,889–15,902.

Riley, P., Luhmann, J., Opitz, A., Linker, J. A., & Mikic, Z. (2010). Interpretation of the cross-correlation function of ACE and STEREO solar wind velocities using a global MHD Model. *Journal of Geophysical Research*, *115*, A11104. https://doi.org/10.1029/2010JA015717

Rosenberg, R. L., & Coleman, P. J. (1969). Heliographic latitude dependence of the dominant polarity of the interplanetary magnetic field. *Journal of Geophysical Research*, *74*(24), 5611–5622. https://doi.org/10.1029/JA074i024p05611

Russell, C. T., & McPherron, R. L. (1973). Semiannual variation of geomagnetic activity. *Journal of Geophysical Research*, *78*(1), 92–108. https://doi.org/10.1029/JA078i001p00092

Simunac, K. D. C., Kistler, L. M., Galvin, A. B., Popecki, M. A., & Farrugia, C. J. (2009). In situ observations from STEREO/PLASTIC: A test for L5 space weather monitors. *Annales Geophysicae*, *27*(10), 3805–3809. Retrieved from http://www.ann-geophys.net/27/3805/2009/, https://doi.org/10.5194/angeo-27-3805-2009

Tóth, G., Sokolov, I. V., Gombosi, T. I., Chesney, D. R., Clauer, C. R., De Zeeuw, D. L., et al. (2005). Space weather modeling framework: A new tool for the space science community. *Journal of Geophysical Research*, *110*, A12226. https://doi.org/10.1029/2005JA011126

Temmer, M., Hinterreiter, J., & Reiss, M. A. (2018). Coronal hole evolution from multi-viewpoint data as input for a STEREO solar wind speed persistence model. *Journal of Space Weather and Space Climate*, *8*, A18. https://www.swsc-journal.org/10.1051/swsc/2018007, https://doi.org/10.1051/swsc/2018007

Thomas, S. R., Fazakerley, A., Wicks, R. T., & Green, L. (2018). Evaluating the skill of forecasts of the near-Earth solar wind using a space weather monitor at L5. *Space Weather*, *16*, 814–828. https://doi.org/10.1029/2018SW001821

Turner, D. L., & Li, X. (2011). Using spacecraft measurements ahead of Earth in the Parker spiral to improve terrestrial space weather forecasts. *Space Weather*, *9*, S01002. https://doi.org/10.1029/2010SW000627